

Department of Electrical
and
Computer Systems Engineering

Technical Report
MECSE-19-2006

Diffused and Rib Optical Waveguides for Modulators and
Micro-Ring Resonator Photonic Filters

L.N. Binh

MONASH
UNIVERSITY

DIFFUSED AND RIB OPTICAL WAVEGUIDES FOR MODULATORS AND MICRO-RING RESONATOR PHOTONIC FILTERS

Le Nguyen Binh

Centre for Telecommunications and Information Engineering, Department of Electrical and Computer Systems Engineering, Monash University, Clayton Victoria 3168 Australia

e-mail: le.nguyen.binh@eng.monash.edu.au

Abstract

To achieve efficient design of high speed modulators and switches, especially micro ring resonators, the fabrication of rib-waveguides and diffused waveguide with suitable mode size is essential to minimise total insertion loss (for ring resonator) and also to maximise the overlap integral between the guided optical field and the applied modulating field.

In this paper, we chose FDM to study the quasi-TE and quasi-TM polarised waveguide modes due to its simplicity and plausible accuracy. We have employed the semi-vectorial analysis which automatically takes full account of the discontinuities in the normal electric field components across any arbitrary distribution of internal dielectric interfaces. The eigenmodes of the Helmholtz equation is solved by the application of shifted inverse power iteration method. This method warrants both the mode size and its relevant propagation constant, which are both important parameters to the design of optical waveguide. The grid size is non-uniform to maximise the accuracy of the optical guided modes and their propagation constants. Diffused waveguides and rib waveguides are designed with different parameters to demonstrate the effectiveness of the method and leading to an optimum design of waveguides of optical modulation and micro-ring resonators.

1 Introduction

Ring resonators (RR) have been attracting to the field of photonic signal processing as a versatile photonic building block with many processing and manipulating of photonic wave applications. Two basic configurations of ring resonator are shown in Fig. 1(a) and (b), showing a single ring coupled to one and two bus waveguides, respectively. The fundamental design parameters are the ring cavity length (L_c) and the coupling coefficient between the ring and the bus. Two main classes of applications of these resonators are high order filters using arrays of RR¹. There are optical waveguides coupled into and out of a micro ring waveguides acting as an optical resonator. Within this resonator ring the guiding of lightwaves is so critical to minimize the propagation loss, thus the design of optical waveguides is very important. For optical waveguiding there are typically two types the diffused guides and the rib-guides. The design of these waveguides requires a formulation that would lead to optimum uses of computing resources and accuracy.

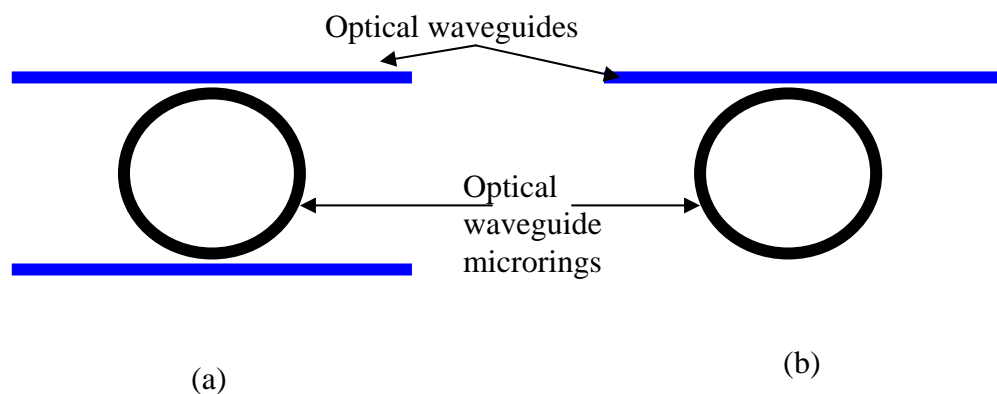


Figure 1 Generic structures of microring resonators

In general, the optical mode of the waveguide is acquired by solving the Helmholtz equation. However, only a few simple waveguide structures can be solved analytically. Therefore, extensive attempts have been made to obtain numerical solutions for a two-dimensional cross section of optical waveguides^[1-17]. One method is the approximate modelling of two-dimensional slab waveguide

¹ Brent Little, Little Optics Inc., USA 2006.

solution successively in both directions, following either the method of Marcatilli^[51] or the effective-index method (EIM)^[34]. However, these methods are not applicable to arbitrarily shaped optical waveguides, neither do they handle waveguide mode near the cutoff region efficiently. A significant number of numerical methods have been proposed to obtain rigorous solutions to the wave equation with pertinent boundary conditions. The popular techniques by far are the finite difference method (FDM)^[4], finite element method (FEM)^[16] or beam propagating method (BPM)^[8]. The application of different techniques based on the above methods such as semivectorial E-field FDM^[6], semivectorial H-field FDM^[47], Rayleigh quotient solution^[46], have been studied and reported. These methods are applicable to arbitrarily shaped optical waveguides. In FEM and FDM, partial differential equations are discretized and then transformed to matrix equations. The calculations of mode indices and optical field distributions are then equivalent to obtaining eigenvalues and eigenfunctions of the coefficient matrices.

In addition to achieve efficient design of high speed modulators and switches, especially micro ring resonators, the fabrication of rib-waveguides and Ti:NbO₃ waveguide with suitable mode size is essential to minimise waveguide insertion loss and also to maximise the overlap integral between the guided optical field and the applied modulating field. Furthermore the bending or radius of curvature is so important for ring resonator to keep the ring size as small as possible. Extensive studies have been devoted in recent decades on fabricating Ti:diffused LiNbO₃ waveguides which couple efficiently to single-mode fibers^[29, 48-51]. A major milestone was achieved when a total fiber-waveguide-fiber insertion loss of 1 dB was achieved for z-cut LiNbO₃ at 1.3 μm ^[50]. Such low loss was achieved by choosing fabrication parameters to yield a relatively deep, clean diffusion, which simultaneously minimised the fiber waveguide mode mismatch loss and the propagation loss. Suchoski and Ramaswamy^[35] has reported on the optimisation of fabrication parameters to obtain Ti:LiNbO₃ single mode waveguides which exhibit both minimum mode size and low propagation loss at 1.3 μm . All these design requirements have led to the significance of the analysis of polarised modes in channel waveguides.

In this paper, we chose FDM to study the quasi-TE and quasi-TM polarised waveguide modes due to its simplicity and plausible accuracy. We have employed the semivectorial analysis^[6, 17, 47] which automatically takes full account of the discontinuities in the normal electric field components across any

arbitrary distribution of internal dielectric interfaces. The semivectorial FDM, despite its simplicity and being free from troublesome spurious solutions, has two major disadvantages of being computational intensive and requiring large amount of memory. Hence, it is necessary to introduce the discretisation scheme on the non uniform mesh, in which mesh intervals can be changed arbitrarily depending on waveguide structures. For this reason, we have modelled the waveguide mode with finite difference method which employs a non uniform discretization scheme^[3,17]. Such a discretization scheme enables us to increase the size of the problem space so that the field component at the boundary can be assumed to have vanished. The grid spacing increases monotonically with increasing distance from the guiding region. The grid lines can also be aligned with the boundaries of the step index changes in conventional structures such as rib, ridge and strip-loaded waveguides as well as quantum well structures. Furthermore, by judiciously placing the grid lines and corresponding cell structure efficiently, we can reduce the required matrix size and hence redundant computer calculations, while preserving the accuracy of the calculations. The non-uniform discretisation scheme also enables us to handle waveguide mode near the cut off region with a relative simple boundary condition. The eigenmodes of the Helmholtz equation is solved by the application of shifted inverse power iteration method. This method warrants both the mode size and its relevant propagation constant, which are both important parameters to the design of optical waveguide.

In the Section 2, we outline the numerical formulation of the non-uniform finite difference scheme as described above. Both quasi-T.E and quasi-T.M polarised mode are addressed. We also assess the accuracy of the numerical result of this scheme by computing the effective refractive index of a few rib and slab dielectric waveguides and compare the results with published results. The effect of grid spacing is also investigated. We will also present the effectiveness of the variable grid spacing in dealing with waveguide mode near the cut off region.

Section 3 describes the modelling of Ti:LiNbO₃ channel waveguide. The effects of various waveguide fabrication parameters such as the diffusion time, diffusion temperature, thickness and width of the titanium strips are studied. The accuracy of the numerical model is assessed by comparing our simulations with experimental and simulation results that are reported in several literatures.

Apart from being able to access the accuracy of the final product of our work, which is the SVMM (Semi-Vectorial Mode Modelling) computer program, we will also present an overview of its application in modelling Ti:LiNbO₃ channel waveguide for optical devices such as modulators and switches.

In essence, this part of this paper work will present an understanding of the numerical formulation involved in the modelling of optical modes in channel waveguides. The robustness of the numerical formulation will enable us to model the optical mode of a channel waveguide with an arbitrary index profile easily and accurately. With recent advancement in computer technology, our work has much to offer in the analysis and design of optical channel waveguides.

2 Non-Uniform Grid Semi-vectorial Polarised Finite Difference Method For Optical Waveguides With Arbitrary Index Profile

2.1 The Propagation Equation

For harmonic wave propagation in the z direction along a rib or channel waveguide, we consider the fields

$$\mathbf{E}(x, y, z) = (E_x, E_y, E_z) \exp j(\omega t - \beta z) \quad (1)$$

$$\mathbf{H}(x, y, z) = (H_x, H_y, H_z) \exp j(\omega t - \beta z) \quad (2)$$

$$\mathbf{D} = \varepsilon(x, y)\mathbf{E}, \quad \mathbf{B} = \mu\mathbf{H} \quad (3)$$

where the dielectric constant $\varepsilon(x, y)$ is piecewise constant and the magnetic permeability μ is completely constant throughout the solution domain. The components of the electric and magnetic fields in Eq (1) are functions of x and y only. Then, applying the Maxwell equations in the magnetic and charge free media and take appropriate algebra we obtain the wave equation:

$$\nabla \times (\nabla \times \mathbf{E}) = \nabla(\nabla \cdot \mathbf{E}) - \nabla^2 \mathbf{E} = \omega^2 \varepsilon \mu \mathbf{E} = k^2 \mathbf{n}^2 \mathbf{E} \quad (4)$$

in which $k = \omega(\epsilon_0\mu_0)^{1/2} = 2\pi / \lambda$ and $\epsilon = \epsilon_0 n^2(x,y)$ with λ being the free space wavelength. With the divergence of $\nabla \cdot \mathbf{D} = 0$ and $\nabla \log_e \epsilon = \nabla \epsilon / \epsilon$, we get

$$\nabla \cdot \mathbf{E} = -\mathbf{E} \cdot \nabla \log_e \epsilon = -\mathbf{E} \cdot \nabla n^2 / n \tag{5}$$

. This may be substituted into (4) to yield the wave equation

$$\nabla^2 \mathbf{E} + k^2 \mathbf{E} + \nabla(\mathbf{E} \cdot \nabla n^2 / n) = 0 \tag{6}$$

As $n(x, y)$ is piecewise constant, $\nabla n^2 / n = 0$ and it should be noted that $\nabla n^2 / n$ is undefined at internal dielectric interfaces where $n(x, y)$ is discontinuous. With the assumption that the fields are polarised either perpendicular (quasi-TM) to or parallel (quasi-TE) to the crystal surface and that the major field components of the modes are perpendicular to the direction of the propagation, Eq (7) can be reduced to

$$(\nabla_T^2 + k^2 n^2) \mathbf{E} = \beta^2 \mathbf{E} \tag{7}$$

in which $\nabla_T^2 = \frac{\partial^2}{\partial x^2} + \frac{\partial^2}{\partial y^2}$, the transverse Laplacian and β is the propagation constant. This is essentially the Helmholtz wave equation.

2.2 Formulation of Non Uniform Grid Difference Equation

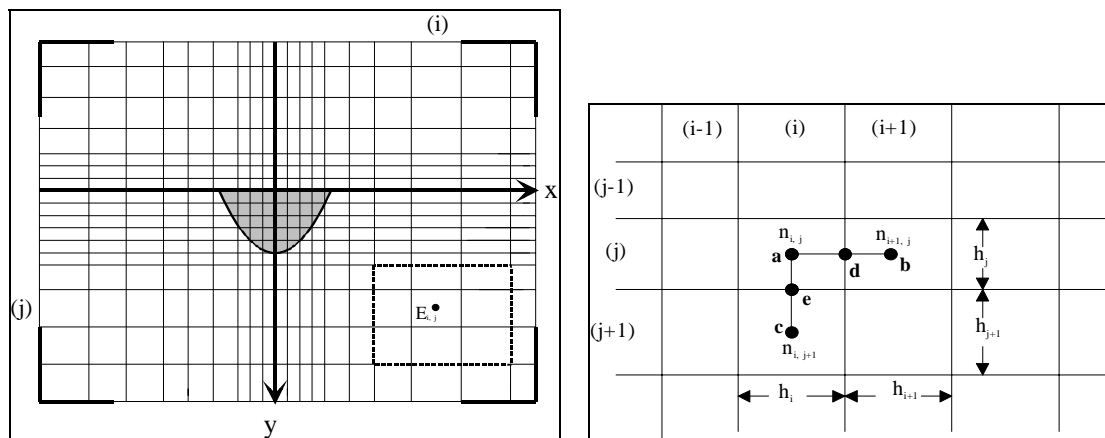


Figure 2: Non uniform discretized grid for FDM scheme (a) and (b) A magnified portion of grid lattice and cell structure of point i, j .

Figure 2(a) shows the grid lines used in the finite difference method formulation. The grid lines are chosen in such a way that denser grids are allocated around the guiding region while coarser grids are assigned to regions further away from the waveguide. Boundaries of abrupt index changes are straddled by the grid lines wherever necessary. Figure 2(b) shows the magnified view of a portion of the grid for a more detailed illustration. Each cell point is located in the center of each rectangular cell. h_i and h_j are the horizontal and vertical grid sizes. The refractive index within each cell is assumed to be uniform. $n_{i, j}$ and $n_{i+1, j}$ represent the values of the refractive index of each small cell as an approximation, which are taken from the continuous refractive index profile $n(x, y)$. Non uniform spacing of the grid lines provides some flexibility in setting up the non uniform grid FDM. The non uniform discretization with increasing spacing away from the guiding region permits sufficient extension of the boundary. This enables us to assume a Dirichlet boundary condition (metal box) where all fields have vanished.

(I) Quasi-TE Mode

For quasi TE polarised mode, E_y is assumed to be zero. E_x is continuous across the horizontal interfaces but discontinuous across vertical interfaces. Therefore, the quasi-TE modes are the eigensolutions of the equation

$$\nabla_t^2 E_x + k^2 n^2 E_x = \beta^2 E_x \quad (8)$$

The discontinuity across the vertical interface will need to be taken into account when formulating the difference equation.

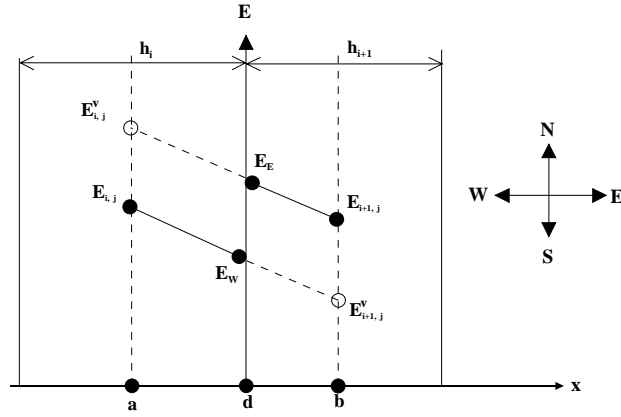


Figure 3: Quasi-TE electric field discontinuity at the boundary between cells (i, j) and cell (i+1, j). Solid lines are the actual field profiles along x axis while $E_{i,j}^v$ and $E_{i+1,j}^v$ are virtual fields.

Figure 3 illustrates the quasi-TE field discontinuity at the boundary between cells (i, j) and (i+1, j). Consider the points a, d and b, with d being at the boundary of the dielectric interface. The horizontal axis is the x-axis while the vertical axis is the electric field amplitude of the respective position of the cell. Assume that the x-axis is pointing towards the east. So, E_E and E_W are the field amplitudes just to the east and the west of the boundary between the cells (i, j) and cell (i+1, j). $E_{i,j}^v$ is the virtual field in cell (i, j) which is the extension of the actual field $E_{i+1,j}$. In other words, $E_{i,j}^v$ is the field seen by the cell (i+1, j). Similarly, $E_{i+1,j}^v$ is the extension of $E_{i,j}$. n_E and n_W are the refractive indices just to the east and the west of the boundary. Since we consider a slowly varying index distribution, we assume that n_E and n_W are approximately equal to $n_{i,j}$ and $n_{i+1,j}$ respectively. The boundary conditions between the cells (i, j) and (i+1, j) are given as follows:

$$n_E^2 E_E = n_W^2 E_W, \Rightarrow n_{i,j}^2 E_E = n_{i+1,j}^2 E_W \quad (9)$$

$$\frac{\partial}{\partial x} E_E = \frac{\partial}{\partial x} E_W = p^+ \quad (10)$$

where p^+ represents the field gradient at the boundary between the cells. We can then use the approximate relationship between $E_{i,j}$, $E_{i+1,j}$, $E_{i,j}^v$, $E_{i+1,j}^v$, and obtain the following equations for E_E and E_W :

$$E_{i+1,j} \approx E_E + (h_{i+1} / 2) \cdot p^+; E_{i,j}^v \approx E_E - (h_i / 2) \cdot p^+; E_{i+1,j}^v \approx E_W + (h_{i+1} / 2) \cdot p^+ \text{ and}$$

$$E_{i,j}^v \approx E_W - (h_i / 2) \cdot p^+ \quad (11)$$

where h_i and h_{i+1} are the horizontal lengths of cell (i, j) and (i+1, j). The four equations above are in fact redundant. Therefore we need only to consider either $E_{i,j}^v$ or $E_{i+1,j}^v$, which we choose $E_{i+1,j}^v$ in our case. The following shows the algebraic manipulation (11):

$$p^+ = 2(E_{i+1,j}^v - E_{i,j}) / (h_i + h_{i+1}); E_{i+1,j}^v = E_{i+1,j} + (E_W - E_E);$$

$$h_{i+1}(E_W - E_{i,j}) = h_i(E_{i+1,j} - E_E) \quad (12)$$

and then

$$E_{i+1,j}^v = \frac{n_{i+1,j}^2(h_i + h_{i+1})E_{i+1} + h_{i+1}(n_{i+1,j}^2 - n_{i,j}^2)E_{i,j}}{(n_{i,j}^2 h_i + n_{i+1,j}^2 h_{i+1})} \quad (13)$$

With similar procedure between cell (i,j) and cell (i+1, j), we can obtain

$$p^- = 2(E_{i,j} - E_{i-1,j}^v) / (h_i + h_{i-1}) \text{ and } E_{i-1,j}^v = \frac{n_{i-1,j}^2(h_i + h_{i-1})E_{i-1,j} + h_{i-1}(n_{i-1,j}^2 - n_{i,j}^2)E_{i,j}}{(n_{i,j}^2 h_i + n_{i-1,j}^2 h_{i-1})}$$

(14)

where p^- is now the field gradient at the boundary between the cells(i-1, j) and (i, j).

Note that the quasi-TE electric field is continuous in terms of y direction even if there are discontinuities in refractive index. Therefore $E_{i,j+1}^v = E_{i,j+1}$, $E_{i,j-1}^v = E_{i,j-1}$

The second derivative can be derived as

$$\frac{\partial^2}{\partial x^2} E_{i,j} = \frac{1}{h_i} [p^+ - p^-] = \frac{1}{h_i} \left[\frac{2(E_{i+1,j}^v - E_{i,j})}{h_{i+1} + h_i} - \frac{2(E_{i,j} - E_{i-1,j}^v)}{h_i + h_{i-1}} \right] \quad (17a)$$

$$\frac{\partial^2}{\partial y^2} E_{i,j} = \frac{1}{h_j} [p^+ - p^-] = \frac{1}{h_j} \left[\frac{2(E_{i,j+1} - E_{i,j})}{h_{j+1} + h_j} - \frac{2(E_{i,j} - E_{i,j-1})}{h_j + h_{j-1}} \right] \quad (15b)$$

Thence we get the discrete wave equation as

$$\begin{aligned} \frac{\partial^2}{\partial x^2} E_{i,j} = & \frac{2n_{i-1,j}^2}{h_i(n_{i,j}^2 h_i + n_{i-1,j}^2 h_{i-1})} E_{i-1,j} + \frac{2n_{i+1,j}^2}{h_i(n_{i,j}^2 h_i + n_{i+1,j}^2 h_{i+1})} E_{i+1,j} \\ & - \left[\frac{2n_{i,j}^2}{h_i(n_{i,j}^2 h_i + n_{i-1,j}^2 h_{i-1})} + \frac{2n_{i,j}^2}{h_i(n_{i,j}^2 h_i + n_{i+1,j}^2 h_{i+1})} \right] E_{i,j} \end{aligned} \quad (16a)$$

$$\frac{\partial^2}{\partial y^2} E_{i,j} = \frac{1}{h_j} \left[\frac{2(E_{i,j+1} - E_{i,j})}{h_{j+1} + h_j} - \frac{2(E_{i,j} - E_{i,j-1})}{h_j + h_{j-1}} \right] \quad (18b)$$

Substituting these into the Helmholtz equation,

$$C_{i-1,j} E_{i-1,j} + C_{i+1,j} E_{i+1,j} - C_{i,j} E_{i,j} + C_{i,j-1} E_{i,j-1} + C_{i,j+1} E_{i,j+1} = \beta^2 E_{i,j} \quad (17)$$

$$\text{Where } C_{i-1,j} = \frac{2n_{i-1}^2}{h_i(n_{i,j}^2 h_i + n_{i-1,j}^2 h_{i-1})}; \quad C_{i+1,j} = \frac{2n_{i+1}^2}{h_i(n_{i,j}^2 h_i + n_{i+1,j}^2 h_{i+1})}; \quad C_{i,j-1} = \frac{2}{h_j(h_j + h_{j-1})};$$

$$C_{i,j+1} = \frac{2}{h_j(h_j + h_{j+1})}; \quad \text{and } C_{i,j} = C_{i-1,j} + C_{i+1,j} + C_{i,j-1} + C_{i,j+1} - k^2 n_{i,j}^2$$

$$(18a)$$

The above equations is essentially an eigenvalue equation of

$$C_{TE} \mathbf{E}_{TE} = \beta_{TE}^2 \mathbf{E}_{TE} \quad (19)$$

in which C_{TE} is a non symmetric band matrix which contains the coefficient of the above equations, β_{TE}^2 is the TE propagation eigenvalue, and \mathbf{E}_{TE} is the corresponding normalised eigenvector representing the field profile $E_x(x, y)$.

(II) *Quasi-TM Mode*

The quasi-TM mode can be formulated in similar fashion. The only difference is that for quasi-TM polarised mode, E_x is assumed to be zero and E_y is continuous across the vertical interfaces but discontinuous across horizontal interfaces. Essentially, the quasi-TM modes are the eigen-solutions of the equation

$$\nabla_t^2 E_y + k^2 n^2 E_y = \beta^2 E_y \quad (20)$$

The detailed derivation of the equation can be found in the literature.^[17] The following are the derivatives and its relevant difference equations:

$$\frac{\partial^2}{\partial y^2} E_{i,j} = \frac{2n_{i,j-1}^2}{h_i(n_{i,j}^2 h_i + n_{i,j-1}^2 h_{j-1})} E_{i,j-1} + \frac{2n_{i,j+1}^2}{h_i(n_{i,j}^2 h_i + n_{i,j+1}^2 h_{j+1})} E_{i,j+1} - \left[\frac{2n_{i,j}^2}{h_i(n_{i,j}^2 h_i + n_{i,j-1}^2 h_{j-1})} + \frac{2n_{i,j}^2}{h_i(n_{i,j}^2 h_i + n_{i,j+1}^2 h_{j+1})} \right] E_{i,j} \quad (21a)$$

$$\frac{\partial^2}{\partial x^2} E_{i,j} = \frac{1}{h_j} \left[\frac{2(E_{i+1,j} - E_{i,j})}{h_{i+1} + h_i} - \frac{2(E_{i,j} - E_{i-1,j})}{h_i + h_{i-1}} \right] \quad (23b)$$

Substituting these into the Helmholtz equation and we get

$$C_{i-1,j} E_{i-1,j} + C_{i+1,j} E_{i+1,j} - C_{i,j} E_{i,j} + C_{i,j-1} E_{i,j-1} + C_{i,j+1} E_{i,j+1} = \beta^2 E_{i,j} \quad (22)$$

$$\text{Where } C_{i-1,j} = \frac{2}{h_j(h_j + h_{i-1})} \quad \text{and } C_{i+1,j} = \frac{2}{h_j(h_j + h_{i+1})}$$

$$C_{i,j-1} = \frac{2n_{i,j-1}^2}{h_j(n_{i,j}^2 h_j + n_{i,j-1}^2 h_{j-1})}; \quad C_{i,j+1} = \frac{2n_{i,j+1}^2}{h_j(n_{i,j}^2 h_j + n_{i,j+1}^2 h_{j+1})} \quad \text{and}$$

$$C_{i,j} = C_{i-1,j} + C_{i+1,j} + C_{i,j-1} + C_{i,j+1} - k^2 n_{i,j}^2 \quad (33e)$$

(III) Eigenvalue Matrix

To solve the difference equation, we need first to discretized the problem space. We assume that the space is sliced into NX pieces along the x direction and NY pieces along the y direction. This will give us

a total of $N (=NX \times NY)$ grid points. The refractive index of each cell is then allocated according to the relevant index distribution.

When the Finite Difference Wave Equations is evaluated at a grid point, say $E_{i,j}$, it will yield a five-point linear equation in terms of the E field of the immediate neighbours, namely $E_{i-1,j}$, $E_{i+1,j}$, $E_{i,j-1}$, $E_{i,j+1}$, each with its relevant coefficient as shown in equations (28) and (33). For a cross sectional area of a waveguide with N such grid points, we would end up with N linearly dependant algebraic equations.

We will now scan through the grid points row after row, at the same time re-labelling the subscripts of E from 1 to N . Consider the original grid point (i, j) . Assuming that the new sequence number is k , then (32) can be rewritten as

$$p_k E_k + l_k E_{k-1} + r_k E_{k+1} + t_k E_{k-Nx} + b_k E_{k+Nx} = \beta^2 E_k \quad (23)$$

where p_k , l_k , r_k , t_k , b_k , are the coefficients $C_{i,j}$, $C_{i-1,j}$, $C_{i+1,j}$, $C_{i,j-1}$, $C_{i,j+1}$, respectively. We can then collect terms and write the equations in a matrix form.

For a 3×3 grid of the refractive index profile, we can write the matrix equations as an the eigenvalue equation of the form $[C].[E] = \beta^2 [E]$ in which $[C]$ is a non symmetric band matrix which contain the coefficient of the above equations, β^2 is the propagation eigenvalue, and $[E]$ is the corresponding normalised eigenvector representing the field profile $E(i,j)$. In the next section we will discuss the approach that we adopt in solving the eigenvalue problem given as

$$\begin{bmatrix} p_1 & r_1 & 0 & b_1 & 0 & 0 & 0 & 0 & 0 \\ l_2 & p_2 & r_2 & 0 & b_2 & 0 & 0 & 0 & 0 \\ 0 & l_3 & p_3 & r_3 & 0 & b_3 & 0 & 0 & 0 \\ t_4 & 0 & l_4 & p_4 & r_4 & 0 & b_4 & 0 & 0 \\ 0 & t_5 & 0 & l_5 & p_5 & r_5 & 0 & b_5 & 0 \\ 0 & 0 & t_6 & 0 & l_6 & p_6 & r_6 & 0 & b_6 \\ 0 & 0 & 0 & t_7 & 0 & l_7 & p_7 & r_7 & 0 \\ 0 & 0 & 0 & 0 & t_8 & 0 & l_8 & p_8 & r_8 \\ 0 & 0 & 0 & 0 & 0 & t_9 & 0 & l_9 & p_9 \end{bmatrix} \begin{bmatrix} E_1 \\ E_2 \\ E_3 \\ E_4 \\ E_5 \\ E_6 \\ E_7 \\ E_8 \\ E_9 \end{bmatrix} = \beta^2 \begin{bmatrix} E_1 \\ E_2 \\ E_3 \\ E_4 \\ E_5 \\ E_6 \\ E_7 \\ E_8 \\ E_9 \end{bmatrix} \quad (24)$$

There are a few major features of the matrix equation above: (i) this type of matrix is often referred to as tridiagonal matrix with fringes. The order of the matrix is $N \times N$, the square of the total number of grid points. Most of terms in the matrix are zeros; (ii) the matrix is non-symmetrical relative to the diagonal term; (iii) the central three diagonal terms always exist and are always non zero; (iv) the coefficients p , l , r , t , b makes up the five bands of the matrix, with p being the main diagonal, l and r being the subdiagonal while t and b the super-diagonal; (v) the subdiagonal diagonal terms are just one term away from the main diagonal while the superdiagonal terms are NX terms away from the main diagonal. The distance between main diagonal and the last non-zero super-diagonal band is commonly referred to as the half bandwidth of a band matrix. (vi) terms such as l_1 , r_N , t_{1-NX} , b_{N-NX} - b_N are missing. This is so since the evaluations of these terms require the E values outside the boundary area, and these values have been assumed zero. Therefore they need not be represented.

2.3 The Inverse Power Method

The properties and characteristics of eigenvalue problem are well known and have been addressed rather extensively in many text book^[18, 19]. This section would only provide a brief overview to highlight the more specific points related to our particular approach.

An $N \times N$ matrix A is said to have an *Eigenvector* x and a corresponding *eigenvalue* λ if the following condition is satisfied:

$$A \cdot x = \lambda x \quad (25)$$

There can be more than one distinct eigenvalue and eigenvector corresponding to a given matrix. The zero vector is not considered to be an Eigenvector at all. The above equation holds only if

$$\det|A - \lambda I| = 0 \quad (26)$$

which is known as the characteristic equation of the matrix. If this is expanded, it becomes an N^{th} degree polynomial in λ whose roots are the eigenvalues. This is an indication that there are always N , though not necessarily distinct, eigenvalues. Equal eigenvalues coming from multiple roots are called degenerate. Root-searching in the characteristic equation however, is usually a very poor computational method for

finding eigenvalues. There are many more efficient algorithms available in locating the eigenvalues and their corresponding vectors.

Unfortunately there is no universal method for solving all matrix type. For certain problems, either the eigenvalues or eigenvectors are needed, while others require both. Furthermore, some problems may only need a small number of solutions out of the total N solutions available, while others need all. To complicate the matter even further, the Eigensolutions could be complex, and some matrices can be so ill-behaved that round off errors in computing can lead to a non-convergence of the solution. Therefore it is of vital importance to be able to choose the right approach in solving an Eigenproblem. Choosing an algorithm often involves the classification of matrix into types like symmetry, non-symmetry, tridiagonal, banded, positive definite, definite, Hessenberg, sparse, random, etc. The matrix in our problem is a non-symmetric banded matrix with bandwidth equal to twice the number of columns in the grid profile. It has great sparsity for most of the elements are zeros. Also, we need only a few eigenvalues that correspond to the guided modes of the waveguide. In other words, there are only a limited number of guided modes, hence the number of eigenvalue λ . The number of Eigensolutions required is small compared with the size of the matrix (often in the order of tens of thousands). All these different factors have led to the choice of the approach called the Inverse Iteration Method^[18,19].

The basic idea behind the inverse iteration method is quite simple. Let \mathbf{y} be the solution of the linear system

$$(\mathbf{A} - \tau \mathbf{I}) \cdot \mathbf{y} = \mathbf{b} \quad (27)$$

where \mathbf{b} is a random vector and τ is close to some eigenvalue λ of \mathbf{A} . Then the solution \mathbf{y} will be close to the eigenvector corresponding to λ . The procedure can be iterated: replace \mathbf{b} by \mathbf{y} and solve for a new \mathbf{y} , which will be even closer to the true eigenvector. We can see why this works by expanding both \mathbf{y} and \mathbf{b} as linear combinations of the eigenvectors \mathbf{x}_j of \mathbf{A} :

$$\mathbf{y} = \sum_j \alpha_j \mathbf{x}_j \quad \text{and} \quad \mathbf{b} = \sum_j \beta_j \mathbf{x}_j \quad (28)$$

Then we have

$$\sum_j \alpha_j (\lambda_j - \tau) \mathbf{x}_j = \sum_j \beta_j \mathbf{x}_j$$

so that

$$\alpha_j = \frac{\beta_j}{\lambda_j - \tau} \text{ and } \mathbf{y} = \sum_j \frac{\beta_j \mathbf{x}_j}{\lambda_j - \tau} \quad (30)$$

If τ is close to λ_n , say, then provided β_n is not accidentally too small, \mathbf{y} will be approximately \mathbf{x}_n , up to a normalisation. Moreover, each iteration of this procedure gives another power of $\lambda_j - \tau$ in the denominator of (43). Thus the convergence is rapid for well-separated eigenvalues.

Suppose at the i^{th} stage of iteration we are solving the equation

$$(\mathbf{A} - \lambda_i \mathbf{I}) \cdot \mathbf{y} = \mathbf{x}_i \quad (31)$$

where \mathbf{x}_i and λ_i are our current guesses for some eigenvector and eigenvalue of interest (we shall see below how to update λ_i). The exact eigenvector and eigenvalue satisfy

$$\mathbf{A} \cdot \mathbf{x} = \lambda \mathbf{x} \rightarrow (\mathbf{A} - \lambda_i \mathbf{I}) \cdot \mathbf{x} = (\lambda - \lambda_i) \mathbf{x} \quad (32)$$

Since \mathbf{y} of (31) is an improved approximation to \mathbf{x} , we normalise it and set

$$\mathbf{x}_{i+1} = \frac{\mathbf{y}}{|\mathbf{y}|} \quad (33)$$

We get an improved estimate of the eigenvalue by substituting our improved guess \mathbf{y} in (33). By (34), the left-hand side is \mathbf{x}_i , so calling λ our new value λ_{i+1} , we find

$$\lambda_{i+1} = \lambda_i + \frac{|\mathbf{x}_i|^2}{|\mathbf{x}_i \cdot \mathbf{y}|}$$

Although the formulas of Inverse Iteration Method seems to be rather straight forward, the actual implementation can be quite tricky. Most of the computational load occurs in solving the linear system of equations. It would be advantageous if we can solve (44) quickly. It is to be reminded that the size of the matrix in our case is dependant upon the total grid size of the problem space. For a typical grid size of 100 by 100 for example, the coefficient matrix would be of size 10,000 by 10,000. The core memory required in a digital computer to store the entire matrix would be phenomenal. Linear system solver such as routine that are available in LINPACK employs a common LU factorisation (Gaussian elimination) plus backward substitution combination algorithm, much like the manual way of solving linear equations. There is an extensive coverage on this topic in most numerical text books^[19]. We will therefore not discuss it further except to mention that the LU factorisation needs only to be done before the first iteration. When the iteration starts, we already have the steps involved in elimination stored away in an array and only backward substitution is necessary. This approach, even with a storage optimised mode in the LINPACK routine still has a storage requirement of about $3 \times (\text{Bandwidth of matrix} \times \text{matrix size})$. Even though this would mean a considerable reduction in memory storage, it still amounts to a rather substantial memory size.

Also, the preconditioner that employs the Incomplete Cholesky Conjugate Gradient Method^[20] and the Orthomin^[20] accelerator have been found to be most stable and converges most quickly for our matrix. On average, the combination of the preconditioner and accelerator enable us to complete a simulation of a typical waveguide in 3 to 5 minutes on a DECApha 3000/300L workstation. The same simulation that incorporates the LINPACK LU decomposition routine would take 25 minutes on the same computer with substantially greater amount of memory. Since the zero elements are no longer involved in the calculations, it is understandable that the NSPCG iterative method will perform more efficiently.

By incorporating NSPCG numerical solver and the Inverse Iterative Method, we have successfully implemented a Mode Modelling Program, SVMM(Semi Vectorial Mode Modelling) capable of modelling channel waveguide of an arbitrary index profile. The Inverse Iterative Method also enables us to model the higher order modes that are supported by the waveguide structure.

3 SVMM Mode Modelling

In every finite difference approach, a few approximations are made and will therefore introduce some error into the final result. The following are a few approximations that are likely to introduce some error in our calculation: (i) The approximation of the full vectorial wave equation by the semivectorial one. (ii) The replacement of the differential equation with the difference equations. (iii) Discretisation error. (iv) Round off error. (v) The error that are introduced by the NSPCG numerical solver itself.

To assess the accuracy, capability and limitation of our program, we have calculated fundamental mode indices of three well-known rib waveguide that are often used as waveguide modeling benchmark. Results of polarised modes have been published^[4-16]. The geometry of the rib waveguide is shown in Figure 4. Parameter include width of the rib w , height of the rib h , thickness of the guiding layer underneath the rib d , index of the substrate n_s and index of the guiding layer n_g are listed in Table 1. The refractive index of the air cladding region, n_c is unity.

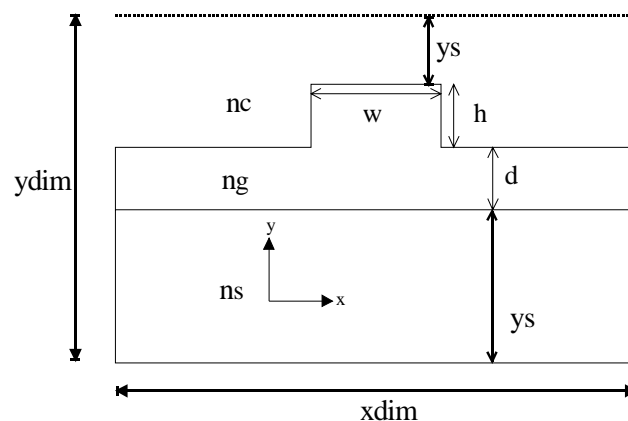


Figure 4 Typical Structure of Rib Waveguide

Guide	n_g	n_s	d (μm)	h (μm)	w (μm)
1	44	34	0.2	1.1	2
2	44	36	0.9	0.1	3
3	44	435	5	2.5	4

Table 1 Parameters of Rib Waveguide for Calculation Benchmark

The three waveguides each has a different characteristic. Structure 1 has relatively large vertical refractive index steps ($\Delta n = 2.44$ and 0.1) which could, for example, correspond to a GaAs guiding layer bound by air and a $\text{Ga}_{0.75}\text{Al}_{0.25}\text{As}$ confining layer. In the lateral direction, the rib height is large and

the width narrow. This structure, with strong light confinement in both lateral and vertical direction, is useful for curved guides, as radiation loss is minimised. This structure does not allow the application of Effective Index Method because the slab outside the rib is cut-off.

Structure 2 shows a weakly guiding feature. In this case the rib height is much less, allowing the mode to extend laterally. This is particularly useful for directional coupler structures, as strong coupling between adjacent guides will result in short coupling lengths. The guiding layer thickness is made small to give a thin mode shape in the vertical direction, and thus low voltage operation. Essentially, this structure is tightly confined vertically and weakly confined horizontally. Such features enable the application of Effective Index Method^[10,29,34] because the small etch step and large width to height ratio are the conditions of validity of this approximate method.

Structure 3 gives a good coupling to an optical fibre. Insertion loss is a crucial parameter for most waveguide devices, and is determined by propagation loss and losses due to mode mismatch. Fresnel reflection loss is also important, but can be reduced to insignificant levels by using $\lambda / 4$ anti-reflection coatings. Mode profiles of a circularly symmetric optical fibre and a waveguide will, in general, be different, due to the differing refractive indices of the semiconductor and the fibre, and also the differing shapes of the modes. The effects of both these factors may be alleviated by the use of appropriate waveguide designs. In structure 3 the guiding layer is relatively thick, and the stripe width and height are adjusted to give a more symmetric mode shape. In this structure the slab mode is near cut-off. Again, it is also to be pointed out that because the rib height is nearly twice the slab thickness and the rib width is less than the rib height, the accuracy of the effective index method is expected to be poor. **Figure 5**,

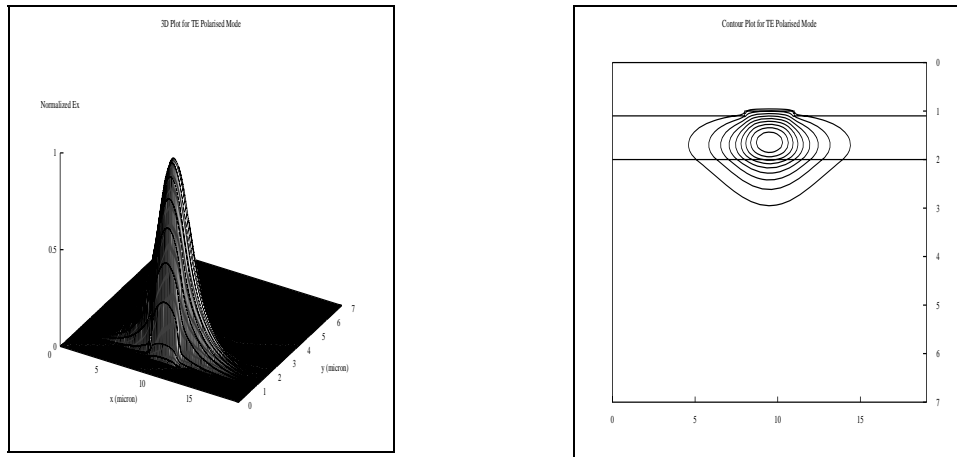


Figure 6 and Figure 7 are the contour plot and 3-D plot of the TE polarised mode of the three waveguide structure calculated by our SVM program.

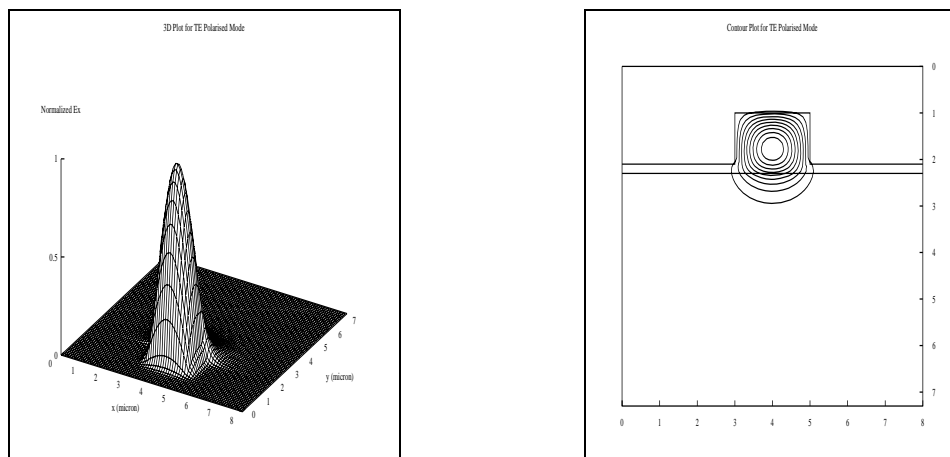


Figure 5(a): 3 dimensional plot of TE polarised mode profile for Waveguide Structure 1 (b): Contour plot of TE polarised mode profile for Waveguide Structure 1

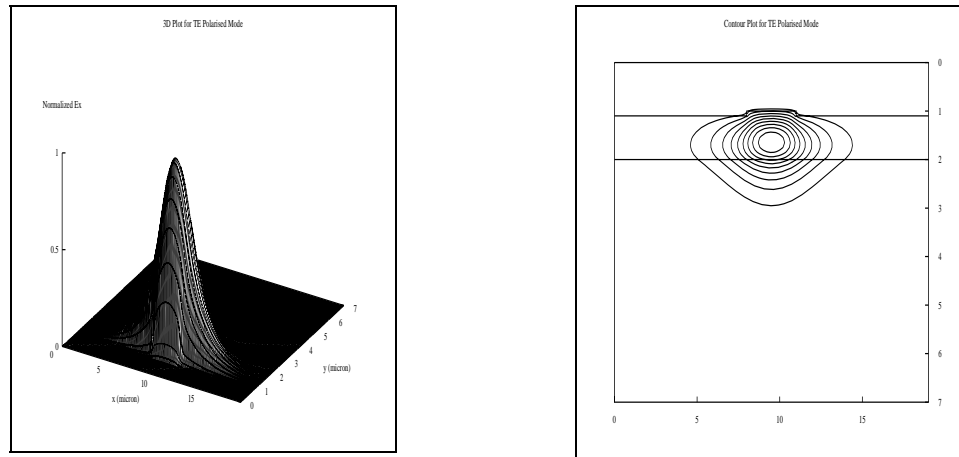


Figure 6 (a): 3 dimensional plot of TE polarised mode profile for Waveguide Structure 2 (b): Contour plot of TE polarised mode profile for Waveguide Structure 2

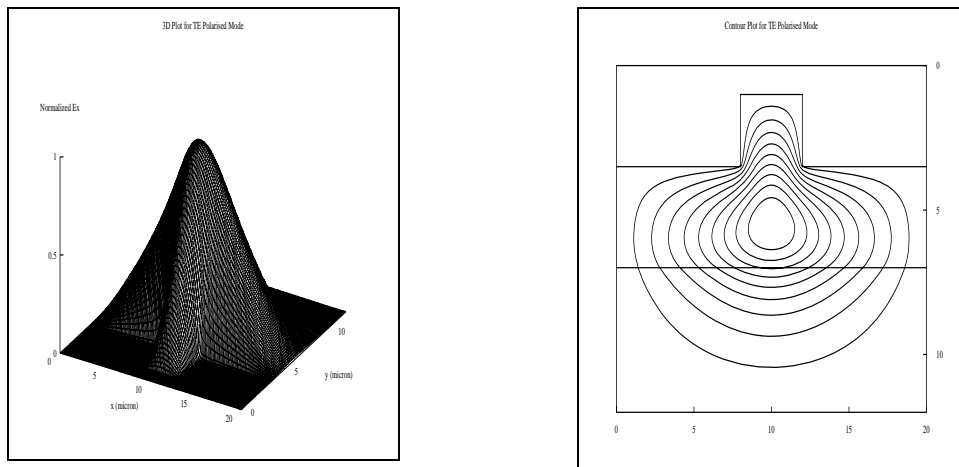


Figure 7 (a): 3 dimensional plot of TE polarised mode profile for Waveguide Structure 3 (b): Contour plot of TE polarised mode profile for Waveguide Structure 3

The grid size h_x and h_y are 0.1. Since we assume that the field value around the computational boundary is zero, it would mean that we require a much larger computational window for both structure 2 and structure 3 so that the assumption would be valid. This however would mean that we either use a coarser grid which will mean a deterioration in accuracy, or maintaining the grid size but face up with a huge eigen matrix to solve. For that reason, the variable grid size comes in handy. We can avoid severe

storage penalty by judiciously placing the denser mesh around the area the higher field value are assume and coarser mesh at region of a much lower field value. This would thus allow us to extend the boundary of the computation without incurring severe storage problem while preserving the accuracy of the computation. The choice of grid size and its influence on the accuracy of the final results would be discussed shall be illustrated in the next section.

1 Choice of Grid Size

A judicious choice of grid size is rather to produce a plausible simulation result. To assess the effect of grid size on the accuracy of our simulation program, we compute the effective index for the TE polarised mode of structure 1 by varying the grid size in both x and y direction, namely h_x and h_y . We compare our result with the one simulated by P. Lusse *et al.* ^[5] which uses a dense mesh of 508×394 mesh points their Full Vectorial Finite Difference Method.

Sim #	h_x (μm)	h_y (μm)	xdim (μm)	ydim (μm)	Total Grid	Effective Index
1	0.5	0.1	8.0	7.3	16×73	3913474
2	0.25	0.1	8.0	7.3	32×73	3899896
3	0.125	0.1	8.0	7.3	64×73	3895512
4	0.1	0.1	8.0	7.3	80×73	3894906
5	0.05	0.1	8.0	7.3	160×73	3894048
6	0.025	0.1	8.0	7.3	320×73	3893836
7	0.025	0.05	8.0	7.3	320×146	3888583
8	0.025	0.025	8.0	7.3	320×292	3887148
9	0.0-2.0 : 0.1 2.0-2.5 : 0.05 2.5-0 : 0.025 0-4.0 : 0.05 4.0-5.5 : 0.025 5.5-6.0 : 0.05 6.0-8.0 : 0.1	0.0025	8.0	7.3	240×292	3887162
10	0.0-2.0 : 0.1 2.0-2.5 : 0.05 2.5-0 : 0.025 0-4.0 : 0.05 4.0-5.5 : 0.025 5.5-6.0 : 0.05 6.0-8.0 : 0.1	0.0-4.0 : 0.025 4.0-7.3 : 0.05	8.0	7.3	240×226	3887165
P. Lusse	-	-	-	-	508×394	88687

Table 2: Calculation of Effective Index with different choice of grid size.

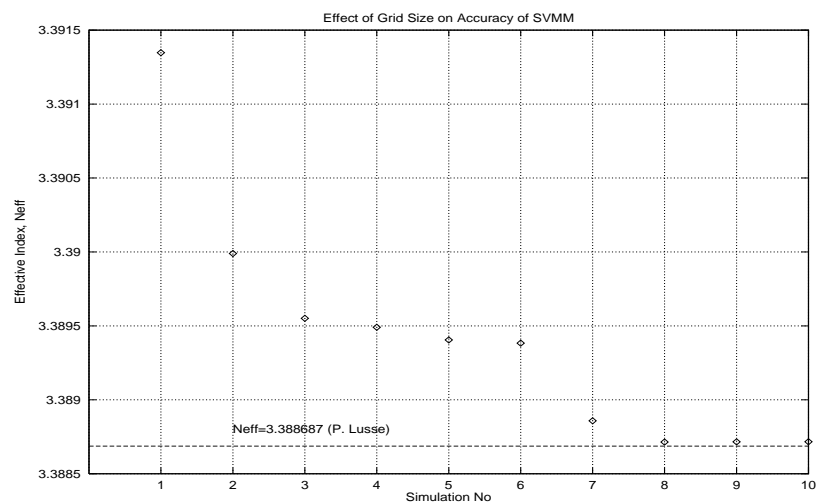


Figure 8 : Refractive index variation with grid size.

In simulation 1 to 6, we keep a constant value of $h_y=0.1$ while reducing h_x from 0.5 down to 0.025. As we can see, as h_x reaches 0.025, we can no longer get a significant improvement on the accuracy. Further reduction of grid size down to 0.01 would be highly impractical because we would end up with 800 grid points along the x direction, thus paying a high penalty in terms of computer memory. In simulation 7-9, we keep h_x at 0.025 while reducing h_y from 0.1 down to 0.025, another significant improvement in accuracy is shown and the results get very close to the one simulated by P. Lusse *et al.* With both h_x and h_y equal to 0.025, a grid size of 320×292 , the difference of our calculated effective index with that of P.

Lusse *et al* is 2.78×10^{-5} . Simulation 10 and 11 shows how the non-uniform scheme could economise storage usage while preserving the desired accuracy. By placing denser grid mesh around the region where higher field values would assumed and coarser mesh for region further away, we manage to reduce our mesh size from 320×292 down to 240×226 (a total reduction of 39200 points) without significant loss in accuracy as can be seen from the graph. The non uniform grid allocation scheme has in this particular case shown its usefulness. (It is to be reminded that each reduction of grid size need to be multiplied by 26 for that is that is the amount of workspace required by the coefficient matrix, eigenvector and the NSPCG numerical solver).

2 Numerical Results

The following tables shows the result of the propagation constants of both TE and TM polarised mode for all three waveguides. The results are compared with several published results. The bolded entries of the tables are results of our work. We can see from the tables that our results compares favourably with all the other published results.

Table 3:

Comparisons of Effective Indices and Normalized Indices at $\lambda=1.55$

Methods	Guide 1		Guide 2		Guide 3	
	n_{eff}	b	n_{eff}	b	n_{eff}	b
SVMM	3887148	0.4835	3953612	0.4391	4368918	0.3782
Sv-BPM ^[8]	388711	0.4834	395471	0.4405	436805	0.3608
Helmholz ^[9]	388764	0.4839	395560	0.4416	436808	0.3614
SI ^[13]	38874	0.4837	39506	0.4354	43688	0.3759
SV ^[47]	3869266	0.4656	3954	0.4401	4368112	0.3621
FD ^[46]	3882623	0.4789	3952147	0.4373	436804	0.3611

a) TE Polarised Mode

Methods	Guide 1		Guide 2		Guide 3	
	n_{eff}	b	n_{eff}	b	n_{eff}	b
SVMM	3879173	0.4755	390647	0.3803	4368434	0.3685
Sv-BPM ^[8]	387924	0.4756	390693	0.3809	436772	0.3543
Helmholz ^[9]	387990	0.4762	390712	0.3811	346772	0.3543
SI ^[13]	38788	0.4752	39032	0.3763	43684	0.3669
SV ^[47]	3867447	0.4638	3905927	0.3796	4367719	0.3542
FD ^[46]	3875430	0.4718	3905701	0.3794	4367751	0.3549

b) TM Polarized Mode

The numerical results that have been presented so far given us an indication of the order of accuracy of the SVMM programs. From these results, we can see that the results presented by our work compares well with other published results. In other words, we are in the position to apply our program to model waveguides of a different index profile.

2 Higher Order Modes

In our earlier discussion, we indicated that the Inverse Power Method can be used to work out the other eigenmodes of the waveguide. To illustrate that, we simulate the waveguide mode of the waveguide structure published by Rahman and Davies^[16]. Table 4 outlines the parameters of the waveguide structure. **Figure 9** and **Figure 10** shows the fundamental mode and the leading asymmetric mode of the TE polarised field.

Table 4: Parameters of rib waveguide of ref^[16] ($\lambda=1.15\mu\text{m}$)

Guide	n_g	n_s	d (μm)	h (μm)	w (μm)
Ref ^[16]	44	40	0.5	0.5	3

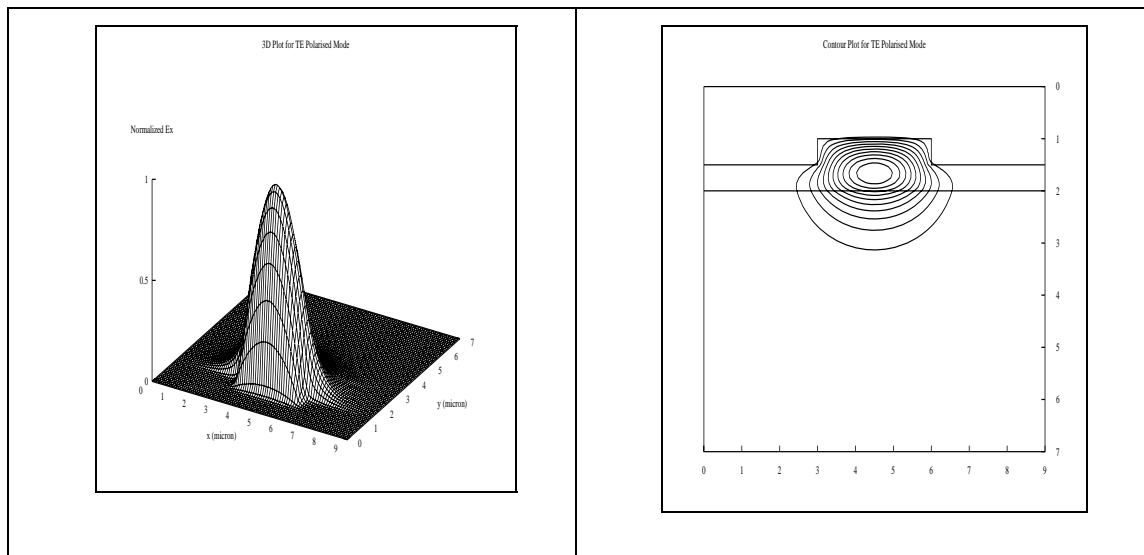


Figure 9(a): 3-D Plot of Fundamental mode of waveguide from ref^[16]. The calculated effective index = 4133105 (b)

Contour Plot of the fundamental mode of the waveguide from ref^[16]

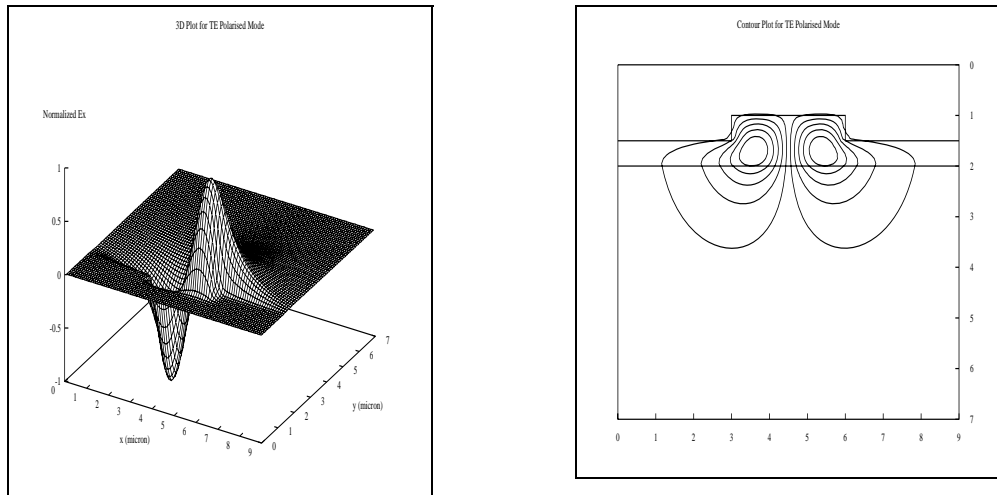


Figure 10(a): 3-D Plot for the Leading Asymmetric Mode of Waveguide in Ref^[16]. Calculated effective index=4025302 (b): Contour Plot of Leading Asymmetric Mode of Waveguide in Ref^[16].

The leading asymmetric mode of **Figure 10** can be obtained with an initial eigenvalue that is close to the eigenvalue of the leading asymmetric mode. A good strategy to acquire a good initial guess for an independent eigenvalue is by perturbing the last few significant digits of the last calculated eigenvalue. In our case, the eigenvalue of the fundamental mode (see **Figure 9**) was calculated to be 347.78889. We then proceeded to the calculation of the asymmetric mode with an initial guess of 346. Other eigenmode can also be worked out in similar fashion. However, we need to remember that there is only a limited number of eigenmode that supported by certain waveguide structure. A good indication that the particular eigenmode is physically not feasible is an effective index which is lower than that of the refractive index of the substrate, thus giving a negative value of the normalized index. This is illustrated in Figure 11.

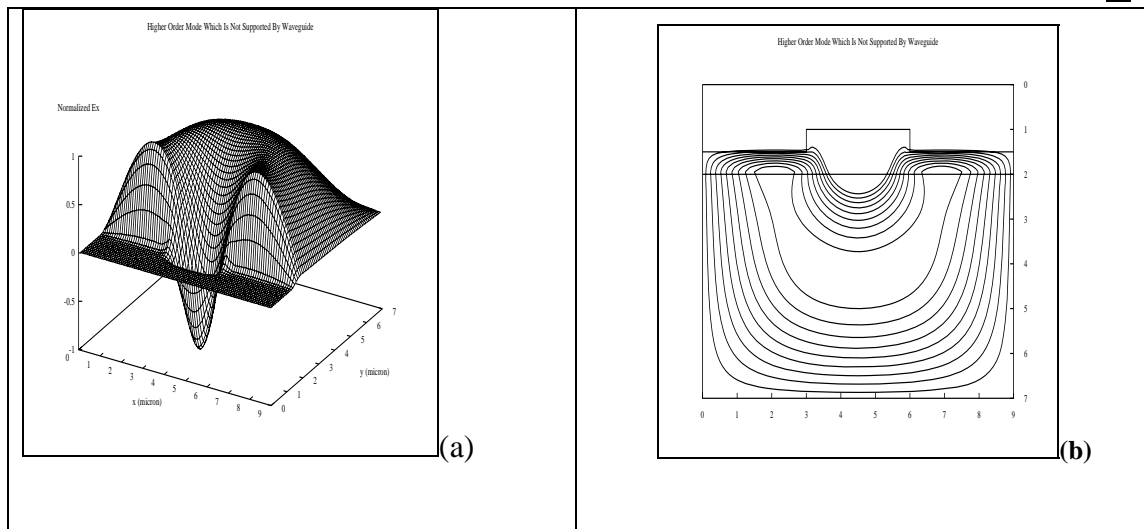


Figure 11(a) 3-D Plot of the third Order Mode which is not supported by the waveguide structure. Calculated effective index = 3980958, Normalised Index=-0.047314 (b) Contour plot of radiated mode

The result shown in Figure 11 is acquired by further reducing the initial guess of the eigenvalues from 346 to 345. As a result of that, we get an effective index of 398 which is lower than the refractive index of the substrate which is 40 in this case. This results in a normalized index b of -0.047. As shown in the contour plot, most of the field is radiated into the substrate of the waveguide.

This feature of SVMM that enables us to work out the higher order modes is extremely important to find out if the designed waveguide can support multimode operation. We will see in the next section how such a feature can be exploited in the design of single mode waveguide.

So far, we have demonstrated how SVMM can be used to simulate rib waveguide. We have simulated a few rib waveguide structures which have been known to be the benchmark structures for accuracy assessment. We have also compared our work with several published results and confirmed the accuracy of our simulation model. We have also illustrated the ability of SVMM to solve for the higher order mode of a given waveguide. All these features would be employed to model the optical mode of the Ti:LiNbO_3 waveguide in the next section.

5 Conclusion

In this paper, we have successfully developed a computer program that carries out a numerical model which is based on a Semivectorial Finite Difference analysis to solve the Helmholtz equation. The

numerical model that we have formulated is capable of modelling the guided modes in optical waveguides of any arbitrary index profile. A non-uniform mesh allocation scheme is employed in the formulation of the difference equations to free more computer memory for the computation of waveguide regions that bear greater significance. The accuracy of our computer program, SVMM is assessed by computing the propagation constants and the effective indices of several rib waveguides that have been known to be excellent benchmark waveguide structures. The results of our computation have compared favourably with other published results^[8,9,13,46,47]. We then continue to simulate the optical guided modes of diffused optical waveguides in LiNbO₃. Our computed mode sizes is consistent with published experimental results. Our simulations however, have shown the inadequacies of the adopted diffusion model for its inability to model the diffused waveguide in a more robust sense. It is suggested that further research to be conducted for a more refine and robust representation of the refractive index profile of Ti:LiNbO₃ diffused waveguide. Despite the shortcoming of the diffusion model that we have adopted, we have demonstrated the potential of SVMM to be used as an analytical and design tool for integrated optical waveguide.

6 References

- [1] K.S Chiang, "Review of numerical and app. roximate methods for the modal analysis of general optical dielectric waveguides", *Optical and Quantum Electronics* **26** S113-S134.
- [2] Saad Michael Saad, "Review of numerical methods for the analysis of arbitrary shaped microwave and optical dielectric waveguides", *IEEE Trans. Microwave Theory and Tech.*, vol. MTT-33, no. 10, October 1985, pp. 894-899.
- [3] S.Seki, *et al.*, "Two dimensional analysis of optical waveguides with a nonuniform finite difference method", *IEE Proceeding-J*, vol. 138, no. 2, April 1991, pp. 123-127.
- [4] M.J. Robertson *et al.*, "Semiconductor waveguides: analysis of optical propagation in single rib structures and directional couplers", *IEE Proceedings*, vol. 132, Pt. J, no. 6, December 1985, pp. 336-342.
- [5] P.Lusse, P.Stuwe, *et al.*, "Analysis of vectorial mode fields in optical waveguides by a new finite difference method", *IEEE Journal of Lightwave Technology*, vol. 12, no. 11, March 1994, pp. 487-49
- [6] M.S Stern, "Semivectorial polarised H field solutions for dielectric waveguides with arbitrary index profiles", *IEE Proceedings*, vol. 135, Pt. J, no. 5, October 1988, pp. 333-338.
- [7] W. Huang and H.A. Haus, "A simple variational app. roach to optical rib waveguides", *Journal of Lightwave Technology*, vol. 9, no. 1, January 1991, pp. 56-61.
- [8] Pao-Lo Liu and Bing-Jin Li, "Semivectorial beam propagation method for analysing polarised modes of rib waveguides", *IEEE Journal of Quantum Electronics*, vol. 28, no. 4, April 1992, pp. 778-782.
- [9] Pao-Lo Liu and Bing-Jin Li, "Semivectorial helmholtz beam propagation by Lanczos reduction", *IEEE Journal of Quantum Electronics*, vol. 29, no. 8, August 1993, pp. 2385-2389.
- [10] T.M. Benson, *et al.*, "Rigorous effective index method for semiconductor rib waveguides", *IEE Proceedings-J*, vol. 139, no. 1, February 1992, pp. 67-70.
- [11] P.C Kendall, *et al.*, "Advances in rib waveguide analysis using weighted index method or the method of moments", *IEE Proceedings*, vol. 137, Pt. J, no. 1, February 1990, pp. 27-29.
- [12] S.V Burke, "Spectral index method app. lied to rib and strip-loaded directional couplers", *IEE Proceedings*, vol. 137, Pt J, no. 1 February 1990, pp. 7-10.
- [13] M.S Stern, "Analysis of the spectral index method for vector modes of rib waveguides", *IEE Proceedings*, vol. 137, Pt. J, no. 1, February 1990, pp. 21-26.
- [14] G. Ronald Hadley and R.E. Smith, "Full vector waveguide modeling using an iterative finite difference method with transparent boundary conditions", *IEEE Journal of Lightwave Technology*, vol. 13, no.3, March 1995, pp. 465-469.
- [15] T.M Benson *et al.*, "Polarisation correction app. lied to scalar analysis of semiconductor rib waveguides", *IEE Proceedings-J*, vol. 139, no. 1 February 1992, pp. 39-41.
- [16] Rahman, and Davies, "Vectorial-H finite element solution of GaAs/GaAlAs rib waveguides", *IEE Proceedings-J*, vol. 132, pp. .349-35

- [17] Chang Min Kim and R.V. Ramaswamy, "Modeling of graded index channel waveguides using non-uniform finite difference method", *Journal of Lightwave Technology*, vol. 7, no. 10, October 1989, pp. 1581-1589.
- [18] Richard L. Burden and J. D Faires, *Numerical Analysis*, 4th edition, PWS-Kent Publishing Company, pp. 492-505.
- [19] William H. Press, *et al.*, *Numerical recipes-the art of scientific computing*, Cambridge University Press, pp. 377-379.
- [20] Thomas C. Opp. *e et al.*, *NSPCG user's guide version 1.0 - a package for solving large sparse linear systems by various iterative methods*, Center for Numerical Analysis, The University of Texas, Austin.
- [21] R.K. Lagu and R.V. Ramaswamy, "A variational finite-difference method for analysing channel waveguides with arbitrary index profiles", *IEEE Journal of Quantum Electronics*, vol. QE-22, no. 6, June, 1986, pp. 968-976.
- [22] E. Strake, *et al.*, "Guided Modes of Ti:LiNbO₃ channel waveguides: a novel quasi analytical technique in comparison with the scalar finite-element method", *IEEE Journal of Lightwave Technology*, vol. 6, no. 6, June 1988, pp. 1126-1135.
- [23] N. Schulz, *et al.*, "Finite difference method without spurious solutions for the hybrid-mode analysis of diffused channel waveguides", *IEEE Trans. Microwave and Tech*, vol. 38, no.6, June 1990, pp. 722-729.
- [24] K.T. Koai and Pao-Lo Liu, "Modeling of Ti:LiNbO₃ waveguide devices: Part I-Directional Couplers", *Journal of Lightwave Technology*, vol. 7. no.3, March 1989. pp. 533-539.
- [25] K.T. Koai and Pao-Lo Liu, "Modeling of Ti:LiNbO₃ waveguide devices: Part II-S-shaped channel waveguide bends", *Journal of Lightwave Technology*, vol. 7. no. 7, July 1989. pp. 1016-1022.
- [26] M. Valli and A.Fioretti, "Fabrication of good quality Ti:LiNbO₃ planar waveguides by diffusion in dry and wet O₂ atmospheres", *Journal of Modern Optics*, 1988, vol. 35, no. 6, 885-890.
- [27] D.S Smith *et al.*, "Refractive Indices of Lithium Niobate", *Optics Communications*, vol. 17, no. 3, June 1976, pp. 332-335.
- [28] D.F Nelson and R.M Mikulyak, "Refractive indices of congruently melting lithium niobate", *Journal of App. lied Physics*, vol. 45, no. 8, August 1974. pp. 3688-3689.
- [29] M. Fukuma and J. Noda, "Optical properties of titanium-diffused LiNbO₃ strip waveguides and their coupling to a fiber characteristics", *App. lied Optics*, vol. 20, no. 4, 15 February 1980, pp. 591-597.
- [30] W.K Burns *et al.*, "Ti diffusion in Ti:LiNbO₃ planar and channel optical waveguides", *Journal of App. lied Physics*, vol.50, no. 10, October 1979, pp. 6175-6182.
- [31] M.D. Feit *et al.*, "Comparison of calculated and measured performance of diffused channel-waveguide couplers", *J. Optical Society of America*, vol.73, no. 10, October 1983, pp. 1296-1304.
- [32] R.C. Alferness *et al.*, "Characteristics of Ti diffused lithium niobate optical directional couplers", *App. lied Optics*, vol. 18, no. 23, 1 December 1979, pp. 4012-4016.
- [33] G.B. Hocker and W.K Burns, "Modes in diffused optical waveguides of arbitrary index profile", *IEEE Journal of Quantum Electronics*, vol. QE-11, no. 6, June 1975, pp. 270-1975.
- [34] G.B Hocker and W.K. Burns, "Mode dispersion in diffused channel waveguides by the effective index method", *App. lied Optics*, vol. 16, no. 1, pp. 113-118.
- [35] P.G. Suchoski and R.V Ramaswamy, "Minimum mode size low loss Ti:LiNbO₃ channel waveguides for efficient modulator operation at 1.3 μm", *IEEE Journal of Quantum Electronics*, vol. QE-23, no. 10, October 1987, pp. 1673-1679.
- [36] M. Minakata, S. Shaito and M. Shibata, "Two dimensional distribution of refractive index changes in Ti diffused LiNbO₃ waveguides", *Journal of App. lied Physics*, vol. 50, no. 5, May 1979, pp. 3063-3067.
- [37] S. Fouchet *et al.*, "Wavelength dispersion of Ti induced refractive index change in LiNbO₃ as a function of diffusion parameters", *Journal of Lightwave Technology*, vol. Lt-5, no. 5, May 1987, pp. 700-708.
- [38] M. Minikata *et al.*, "Precise determination of refractive index changes in Ti-diffused LiNbO₃ optical waveguides", *Journal of App. lied Physics*, vol. 49, no. 9, September 1978, pp. 4677-4682.
- [39] S.K. Korotky, W. J. Minford, *et al.*, "Mode size and method for estimating the propagation constant of single mode Ti:LiNbO₃ strip waveguides", *IEEE Journal of Quantum Electronics*, vol. QE-18, No-10, October, 1982, pp. 1796-1801.
- [40] Murray R. Spiegel, *Mathematical Handbook of Formulas and Tables*, Shaum's Outline Series, McGraw hill Book Company.
- [41] *Properties of Lithium Niobate*, Emis Datareviews Series no.5, INSPEC publication, pp. 131-146.
- [42] Anurag Sharma and Pushpa Bindal, "Analysis of diffused planar and channel waveguides", *IEEE Journal of Quantum Electronics*, vol. 29. no. 1, January, 1993, pp. 150-15
- [43] Anurag Sharma and Pushpa Bindal, "An accurate variational analysis of single mode diffused channel waveguides", *Optical and Quantum Electronics* **24** 1992, pp. 1359-1371.
- [44] Anurag Sharma and Pushpa Bindal, "Variational analysis of diffused planar and channel waveguides and directional couplers", *J. Opt. Soc. Am. A*/vol. 11, no. 8, August 1994, pp. 2244-2248.
- [45] J. Ctyroky, *et al.*, "3-D analysis of LiNbO₃: Ti channel waveguides and directional couplers", *IEEE Journal of Quantum Electronics*, vol. QE. 20, no. 4, April 1984, pp. 400-409.
- [46] M.S Stern, "Rayleigh quotient solution of semivectorial field problems for optical waveguides with arbitrary index profiles", *IEE Proceeding, Pt J, Optoelectronic*. vol. 138, 1990, pp. 185-190
- [47] M.S Stern, "Semivectorial polarised finite difference method for optical waveguides with arbitrary index profiles", *IEE Proceedings*, vol. 135, Pt. J, no. 1, February 1988, pp. 56-6
- [48] C.Bulmer, *et al.*, "High efficiency flip-chip coupling between single mode fibers and LiNbO₃ channel waveguides", *App. lied Physics Letter*, vol. 37, 1981, pp. 351-35
- [49] V. Ramaswamy, *et al.*, "High efficiency single mode fiber to Ti:LiNbO₃ waveguide coupling", *Electronic Letter*, vol. 10, 1982, pp. 30-31.
- [50] R.C. Alferness, *et al.*, "Efficient single mode fiber to titanium diffused lithium niobate waveguide coupling for λ=1.32μm", *IEEE Journal of Quantum Electronics*, vol. QE-18, 1982, pp. 1807-181
- [51] E.A.J. Marcatilli, "Dielectric rectangular waveguide and directional couplers for integrated optics", *Bell Syst. Tech. J.*, 1969, **48**, pp. 2071-2102.